Neural Computing and Applications (2023) 35:23465–23476
https://doi.org/10.1007/s00521-021-06039-x

SPECIAL ISSUE ON HUMAN-IN-THE-LOOP MACHINE LEARNING AND ITS APPLICATIONS

Grid cell modeling with mapping representation of self-motion for path integration

Jiru Wang[1] · Rui Yan[2] · Huajin Tang[3]

Received: 28 November 2020 / Accepted: 13 April 2021 / Published online: 2 February 2022

Abstract
The representation of grid cells in the medial entorhinal cortex region is crucial for path integration. In this paper, we proposed a grid cell modeling mechanism by mapping the agent's self-motion in Euclidean space to the neuronal activity of grid cells. Our representational model can achieve multi-scale hexagonal patterns of grid cells from recurrent neural network (RNN) and enables path integration for 1D, 2D and 3D spaces. Different from the existing works which need to learn weights of RNN to get the vector representation of grid cells, our method can obtain weights by direct matrix operations. Moreover, compared with the classical models based on continuous attractor network, our model avoids the connection matrix's symmetry limitation and spatial representation redundancy problems. In this paper, we also discuss the connection pattern between grid cells and place cells to demonstrate grid cells' functioning as a metric for coding space.

Keywords Path integration · Grid cell · Recurrent neural network · Jacobian matrix

1 Introduction

Many species can keep track of their own position without environmental cues and navigate based completely on self-motion information, which is called path integration [18, 27]. The discoveries of spatial sensitive neurons, such as place cells and grid cells, show us spatial cognition may arise from neural activity of these neurons. Exploring how they represent Euclidean space is the key to knowing the brain's representation and encoding for space-related tasks.

✉ Rui Yan
Ryan@zjut.edu.cn

Jiru Wang
wangjr0722@nudt.edu.cn

Huajin Tang
htang@zju.edu.cn

[1] College of Meteorology and Oceanography, National University of Defense Technology, Changsha 410073, China

[2] College of Computer Science and Technology, Zhejiang University of Technology, Hangzhou 310023, China

[3] College of Computer Science and Technology, Zhejiang University, Hangzhou 310027, China

Grid cells have been kept in focus in spatial cognition research field, which are considered as path integrators in brain [7, 19, 25]. They help animals to estimate spatial position based on self-motion in the absence of external cues, supporting navigation, spatial memory and other high-level cognitive processes [14, 30]. Grid cells have distributed hexagonal firing patterns covering the environment explored by the animal. A grid cell is characterized by three parameters: spatial scale (the distance between centers of two neighboring firing fields), orientation (the angle between the line joining two neighboring firing fields and a reference axis) and phase (the distance between a specific reference point and the center of the firing field closest to this point) [12, 17], as shown in Fig. 1. Grid phase appears to be organized non-topographically [17] and spatial scale discretely increases from dorsal to ventral MEC [29]. Grid cells are functionally organized into different modules and cells in the same module have the same scale but different phases. For each pair of successive modules, the larger scale can be obtained by multiplying the smaller scale by a factor. This way of grid cell organization may be the optimal way to represent space at

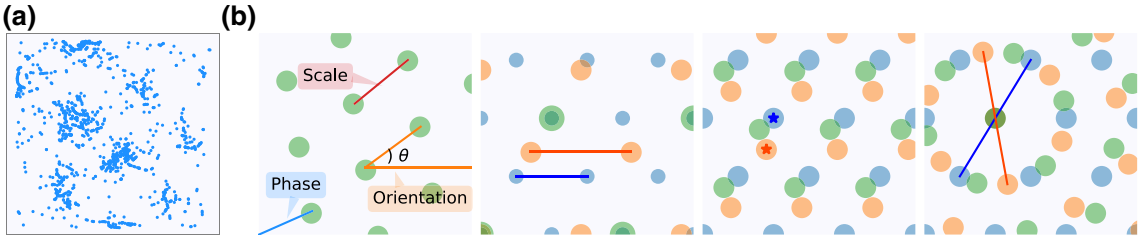

Fig. 1 Spatial firing patterns of grid cells. **a** The firing pattern of a specific grid cell from the neuroscience experiment (data from http://www.ntnu.edu/kavli/research/grid-cell-data). **b** First column, schematic of grid cell (green circle), being defined by spatial scale, phase and orientation. The next three columns, three grid cells (green, orange and blue circle) with different spatial scales, phases and orientations (color figure online)

maximal resolution with the minimum number of grid cells [21, 31].

Many models have been proposed to account for grid cell's hexagonal firing pattern. What they have in common is that the distributed pattern arises from path integration driven by incoming velocity signals from the agent's self-motion in space [25]. Generally speaking, grid cell can be modeled at the single-cell level or network level, depending on whether recurrent interactions between grid cells exist. Oscillatory interference (OI) models are classical single-cell models [4], which have been challenged by further research with other animals except for rats [33]. Animal's motion states, such as the linear velocities, angular velocities and accelerations, may change in different environments. These fluctuations may lead to a problem for the single-cell based models: the relative difference (such as phase) between neighboring grid cells' spatial firing patterns can hardly stay the same across different environments. CAN-based models are classical network models in which grid cells are recurrently connected based on short-range excitation and global inhibition [3, 16]. Driven by velocity input, activity bumps form spontaneously and move smoothly on the grid neural sheet and then path integration is done [11, 23, 32]. The problem of CAN-based models is the strong assumption about the wiring between grid cells in the network and they cannot explain the non-topography of spatial phases in the grid cell population. Moreover, many grid cells in CAN share identical firing patterns, which means that their activity level will maintain the same for all time. Here, it is called spatial representation redundancy, as shown in Fig. 2. For the same spatial area, CANs with smaller spatial scales have more representation redundancy.

Recently, researchers try to simulate animals' spatial behaviors through artificial intelligence techniques [1, 6]. Specifically, with movement-related velocity signals, a recurrent neural network (RNN) is trained to perform self-localization in a virtual space and grid-like neuronal representation emerges within the network, similar to grid cells' hexagonal firing patterns observed in rodent's brain. These training-based models show us the potential of using artificial intelligence to test theories about the spatial cognition mechanism in brain. In addition, Gao et al. proposed a representational model for grid cells, in which the agent's self-position is represented by a high-dimensional vector and the displacement is represented by a matrix that transforms the vector [13]. The movement from the current position to the next position is modeled by matrix-vector multiplication. The angle between two nearby vectors equals the Euclidean distance between the two corresponding positions multiplied by a magnifying factor. The inner product between two vectors measures the adjacency between the two corresponding positions, which is defined by a kernel function of the Euclidean distance between the two positions. This representational model has explicit algebra and geometry, being able to learn hexagon patterns of grid cells, do path integral and path planning. Ben et al. provide an analytic theory that unifies previous perspectives about grid cell firing by casting the learning dynamics of neural networks trained on navigational tasks as a pattern forming dynamical system, and extend this theory to the case of learning multiple grid maps [28]. This paper unifies previous accounts of grid cell firing and provides a novel framework for predicting the learned representations of recurrent neural networks. These works tend to explore the relationship between grid-like firing patterns and spatial tasks. Inspired by biological grid cells' multi-scale periodic representations, Mai et al. introduce an encoder-decoder framework as a general-purpose space representation model [20]. It is an inductive learning model that can be trained in an unsupervised manner. They conduct two experiments on POI type prediction based on POI locations and nearby POIs, demonstrating the effectiveness of this model. It is suggested that it is the ability to integrate representations of different scales that makes the grid cell models and outperforms previous ML baseline methods. This work focuses on applying the related theoretical results about grid cells to real-world data in geoinformatics.

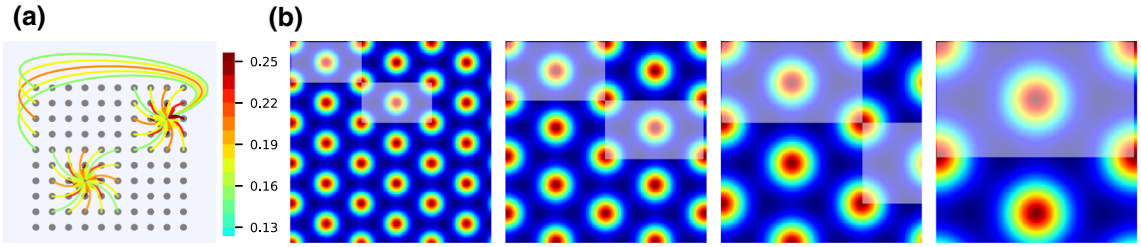

Fig. 2 Continuous attractor network (CAN)-based grid cell modeling. **a** Schematic of local, excitatory weighted connections between grid cells. Darker color means stronger connection. **b** Spatial representation redundancy in CAN. Each column illustrates the heat map of all grid cells' activity at the same time in a CAN. For each heat map, taking grid cells covered by a semi-transparent panel as a unit, they will always have the same activity as grid cells in other units (color figure online)

Besides, a considerable proportion of animals perform daily activities in 3D space, but most models have been done in 2D space. A general grid cell modeling mechanism is required, at the network level, to achieve grid cell modeling for path integration in spaces of different dimensionality. In this paper, we propose a general grid cell modeling mechanism by modeling the mapping from the agent's spatial self-motion to the grid cells' activation. Jacobian matrix $\boldsymbol{J}$, as the mapping representation, is applied to map the agent's self-motion from Euclidean space to neural activity space. Based on our proposed modeling mechanism, representational models of grid cells can be achieved for different dimensions (1D, 2D and 3D) and multi-scale hexagonal firing patterns of grid cells also emerge from RNN. Compared with currently existing models, the proposed modeling mechanism will benefit from the combination of single-cell-based and network-based grid cell modeling. Recurrent connections between grid cells are maintained and the symmetry limitation on connection matrix and spatial representation redundancy in CAN are effectively avoided. Different from existing training-based RNN models, network weights are derived from the mapping of self-motion from Euclidean space to neuronal activity of grid cells, but not high-cost network training. Moreover, it is a general mechanism that can achieve multi-scale grid cell models for path integration in 1D, 2D and 3D spaces.

In addition, we analyze how grid scale and phase distribution exert influence on our model's grid coding performance and then referable modeling instruction is given. We also underline the necessity of grid cells' distance metric ability and work out the spatial position decoding and distance metric mechanism embedded in grid cells' population activity by analyzing connection weights' distribution between grid cells and place cells. With the help of artificial intelligence technique, we provide an instructive way of thinking about how grid cells function as a metric for coding space.

2 The general mechanism for grid cell modeling

When animals move in environment, self-motion information can be integrated through neural activity in brain. Here, a mapping representation is given to map self-motion in Euclidean space to neural activity of grid cells. Jacobian matrix is a very useful tool that has been heavily used in robotic and automation domains to define the dynamic relationship between two different representations in a system. The path integration in brain can be seen as a mapping from Euclidean space to grid cells' activity space $f : \mathbb{R}^m \rightarrow \mathbb{R}^n$ and the Jacobian matrix $\boldsymbol{J}_f \in \mathbb{R}^{m\times n}$ can be used for the mapping from mD space to nD space. Inspired by this, the mapping from self-motion in Euclidean space to grid cells' activity is completed based on Jacobian matrix and then a general grid cell modeling mechanism is achieved for path integration in 1D, 2D and 3D space. The flow of the general mechanism for grid cell modeling we proposed is given below:

1. Based on biologically plausible characteristics of grid cells discovered in neuroscience, formulaic description $\boldsymbol{s}(\boldsymbol{r}) : \mathbb{R}^m \rightarrow \mathbb{R}^n$ is built to simulate n grid cells' firing patterns, a vector function with respect to the mD Cartesian coordinate $\boldsymbol{x}$ in Euclidean space.
2. According to $\boldsymbol{s}(\boldsymbol{r})$, the Jacobian matrix $\boldsymbol{J}$ can be obtained to complete the mapping from mD Euclidean space to nD vector space of grid cell activity.
3. The grid cell dynamics is achieve based on a recurrent neural network in which recurrent weights can be worked out according to $\boldsymbol{J}$ during the mapping process.

For the simple implementation of grid cell modeling in 1D and 2D space, the modeling details are not included and the network weights' calculation formulas necessary for building the grid cell dynamics will be included in "Appendix 1" and "Appendix 2". In the following part, we will show how to achieve the mapping representation of grid cells for path integration in 3D space.

3 Mapping representation of grid cells

In this section, the proposed grid cell modeling mechanism is illustrated by grid cell modeling in 3D space. The specific implementation will be detailed through three parts: the formulaic description of grid cell's firing pattern, the mapping from self-motion in Euclidean space to neuronal activity of grid cells, and dynamics of grid cells for path integration.

3.1 Formulaic description of grid cells' firing patterns

Although a significant corpus of computational models exists in 2D space[3–5, 16], models of 3D path integration are comparatively fewer. Grid-like firing patterns in 3D space can be formed by stacking multiple layers of hexagonal firing patterns in 2D planes and these layers are composed of three repeated layers with specific shift, called face-centered cubic(FCC) lattice. Since many modeling studies have predicted the possibility of FCC lattice structure for the grids in the 3D space owing to its higher packing fraction[9, 22, 24], FCC lattice structure is used for modeling 3D grid cells in this paper. Since the actual scale, phase and orientation of 3d grid cell have not been empirically confirmed yet, the biological validity of the chosen scale and phase remains to be verified.

N grid cells are included, and the grid cell population's activity is denoted as: $\boldsymbol{s}(\boldsymbol{r}) = [\,s_1, s_2, \ldots, s_N\,]^T$. The formulaic description of the ith grid cell's firing pattern can be formed as the function of 3D spatial position $\boldsymbol{r}(x, y, z)$, as shown below:

$$s_j(\boldsymbol{r}) = \frac{1}{4}\sum_{i=1}^{4}\cos(\boldsymbol{k}_i(\boldsymbol{r} - \Delta\boldsymbol{r}_j))$$
$$\boldsymbol{K} = \begin{bmatrix}\boldsymbol{k}_1\\ \boldsymbol{k}_2\\ \boldsymbol{k}_3\\ \boldsymbol{k}_4\end{bmatrix} = \frac{2\pi}{k_0}\begin{bmatrix}0 & 0 & \sqrt{3/2}\\ 2/\sqrt{3} & 0 & -1/\sqrt{6}\\ -1/\sqrt{3} & 1 & -1\sqrt{6}\\ -1/\sqrt{3} & -1 & -1/\sqrt{6}\end{bmatrix} \tag{1}$$

where $\boldsymbol{k}_i$ is given as the row vector of the matrix $\boldsymbol{K}$, $\Delta\boldsymbol{r}_j = (\Delta x_j, \Delta y_j, \Delta z_j)$ and k_0, respectively, determine the phase and spatial scale of grid cell firing patterns.

According to Eq. (1), $\boldsymbol{s}(\boldsymbol{r})$ can be represented as:

$$\boldsymbol{s}(\boldsymbol{r}) = \boldsymbol{M}\boldsymbol{g}(\boldsymbol{r})$$

where

$$\boldsymbol{g}(\boldsymbol{r}) = [\cos\boldsymbol{k}_1\boldsymbol{r} \quad \cdots \quad \cos\boldsymbol{k}_4\boldsymbol{r} \quad \sin\boldsymbol{k}_1\boldsymbol{r} \quad \cdots \quad \sin\boldsymbol{k}_4\boldsymbol{r}]^T$$
$$\boldsymbol{M} = \frac{1}{4}\begin{bmatrix}\boldsymbol{g}(\Delta\boldsymbol{r}_1)^T\\ \vdots\\ \boldsymbol{g}(\Delta\boldsymbol{r}_N)^T\end{bmatrix}$$

Let $\boldsymbol{M}^\dagger$ denotes the pseudo-inverse matrix of $\boldsymbol{M}$, then:

$$\boldsymbol{g}(\boldsymbol{r}) = \boldsymbol{M}^\dagger\boldsymbol{s}(\boldsymbol{r}) \tag{2}$$

3.2 Mapping from Euclidean space to neural activity

For achieving the mapping from self-motion in Euclidean space to grid cell population activity, Jacobian matrix is expected to be used as the mapping representation, which is a matrix of all first-order partial derivatives of the vector-valued function $\boldsymbol{s}$. With $\boldsymbol{s}(\boldsymbol{r})$: $\mathbb{R}^3 \to \mathbb{R}^N$ and the corresponding Jacobian matrix $\boldsymbol{J} \in \mathbb{R}^{3\times N}$, the following formula is obtained:

$$\frac{\mathrm{d}\boldsymbol{s}}{\mathrm{d}t} = \boldsymbol{J}\frac{\mathrm{d}\boldsymbol{r}}{\mathrm{d}t} = \boldsymbol{J}\boldsymbol{v}_t$$
$$\boldsymbol{J} = \begin{bmatrix}\partial s_1/\partial x & \partial s_1/\partial y & \partial s_1/\partial z\\ \vdots & \vdots & \vdots\\ \partial s_N/\partial x & \partial s_N/\partial y & \partial s_N/\partial z\end{bmatrix} \tag{3}$$

and $\boldsymbol{v}_t = [v_1^t, v_2^t, v_3^t]^T$ is the velocity vector in Euclidean space at time t. Combining with $\boldsymbol{s}(\boldsymbol{r})$ in Eq. (1), $\boldsymbol{J}$ can be worked out:

$$\begin{aligned}\boldsymbol{J} &= [\,\partial\boldsymbol{s}/\partial x \quad \partial\boldsymbol{s}/\partial y \quad \partial\boldsymbol{s}/\partial z\,]\\ &= [\,\boldsymbol{M}\boldsymbol{B}_1\boldsymbol{g}(\boldsymbol{r}) \quad \boldsymbol{M}\boldsymbol{B}_2\boldsymbol{g}(\boldsymbol{r}) \quad \boldsymbol{M}\boldsymbol{B}_3\boldsymbol{g}(\boldsymbol{r})\,]\end{aligned} \tag{4}$$

where

$$\boldsymbol{B}_m = \begin{bmatrix}0 & \boldsymbol{B}_{m1}\\ \boldsymbol{B}_{m2} & 0\end{bmatrix}$$
$$\boldsymbol{B}_{m1} = diag[-K_{1m}, -K_{2m}, -K_{3m}, -K_{4m}]$$
$$\boldsymbol{B}_{m2} = diag[K_{1m}, K_{2m}, K_{3m}, K_{4m}]$$

Combined with Eqs. (2), (4) and (3) can be translated and finally the following formula can be obtained:

$$\mathrm{d}\boldsymbol{s}/\mathrm{d}t = \sum_{i}^{3} v_i^t\boldsymbol{W}^i\boldsymbol{s}$$
$$\boldsymbol{W} = [\,\boldsymbol{M}\boldsymbol{B}_1^1\boldsymbol{M}^\dagger \quad \boldsymbol{M}\boldsymbol{B}_2\boldsymbol{M}^\dagger \quad \boldsymbol{M}\boldsymbol{B}_3\boldsymbol{M}^\dagger\,]$$

3.3 Grid cell dynamics for path integration

The mapping representation $\boldsymbol{J}$ has been introduced for mapping self-motion in Euclidean space to neural activity of grid cells. To organize grid cells through recurrent

connections and complete path integration, the rate-based dynamics of grid cells can be formulated as:

$$\tau \mathrm{d}\boldsymbol{s}/\mathrm{d}t = f\left(\sum_{i=1}^{3} v_i^t \boldsymbol{W}^i \boldsymbol{s}\right) \tag{5}$$

where the activation function $f(x) = 0$ if $x \leq 0$ otherwise $f(x) = 1$.

According to the above dynamical model, grid cells with the same scale but different phases will be organized into a recurrent neural network (a module). A complete grid model can be achieved by the adjustment of k_0, including multiple recurrent neural networks with different spatial scales. Each of the networks is called a sub-module or a sub-RNN.

4 Experiment results

In this section, multi-scale grid cell modeling is done based on the proposed modeling mechanism for path integration in 2D and 3D spaces. A grid model includes several sub-RNNs in which grid cells are organized into a recurrent neural network.

4.1 Grid firing patterns

Two grid cell models are firstly completed, respectively, in 2D and 3D space, which have similar network structures. Both of them include five sub-RNNs with different grid scales for path integration and each network includes a grid cell population with different phases but the same scale.

Velocity signals derived from the agent's random exploration in a 25 m^2 square area (Fig. 3a) as the input, grid cells' spatial firing patterns in 2D space are obtained based on the grid cell dynamics for path integration (Eq. 9). Five grid cells are randomly selected, respectively, from five sub-RNNs with different spatial scales and their spatial activity maps are illustrated in Fig. 3b. In the same way, we also obtain spatial firing patterns of five grid cells randomly selected from the 3D grid cell model, as shown in Fig. 4a.

4.2 Grid coding performance analysis

The grid coding performance means the ability to generate standard hexagonal grid-like firing patterns for grid cells and can be measured by the comparison with ground truth derived from the formulaic description of grid cells. The

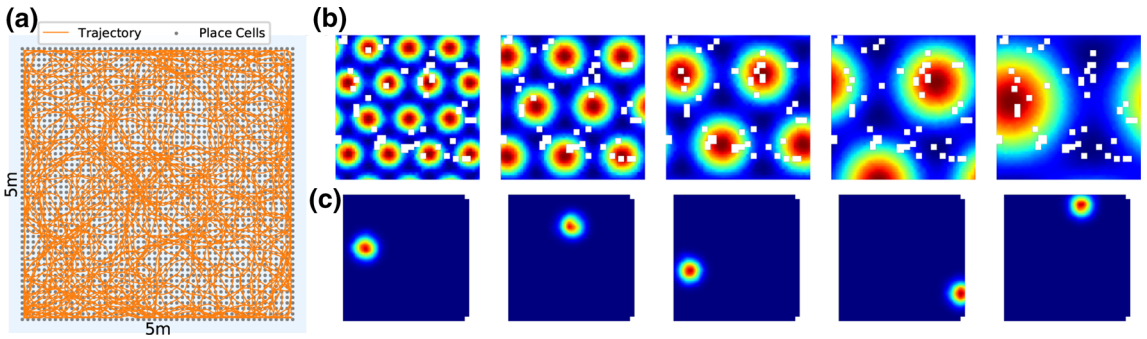

Fig. 3 Exploration of the agent in 2D space. **a** The agent's random exploration in a 25 m^2 area (orange line) and place cells (grey circles) uniformly covering the whole area. **b** Multi-scale spatial activity maps of grid cells. **c** Spatial activity maps of place cells (color figure online)

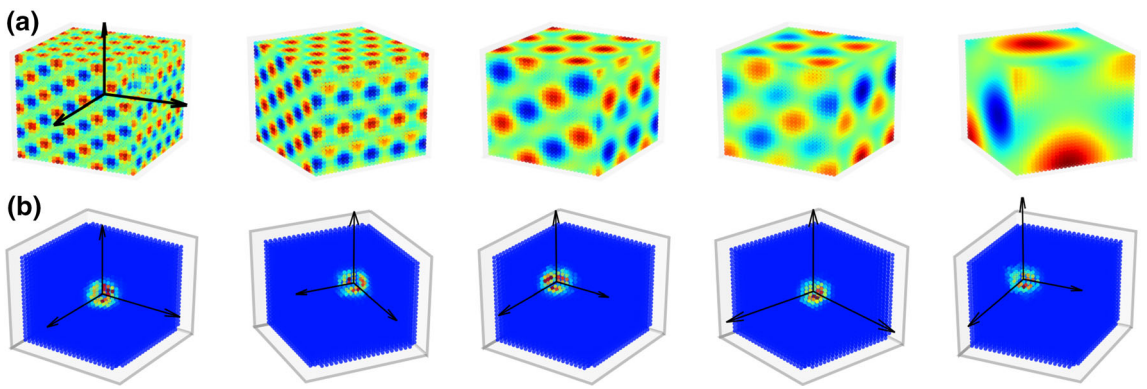

Fig. 4 Grid firing patterns in 3D space. **a** Multi-scale spatial activity maps of grid cells. **b** Spatial activity maps of place cells

grid coding performance is determined by the coding performance of all sub-modules. For each sub-module, in addition to the obvious effect of the number of grid cells on coding performance, the effect of grid scale and phases distribution on coding performance are also analyzed. An indicator AGE quantifying the models' coding performance is defined:

$$\mathrm{AGE} = \frac{1}{N}\sum_{t=0}^{T} \|Gp^t - Gg^t\|$$

which is all grid cells' average of accumulated grid coding error during exploration. N is the number of grid cells involved, $Gp^t = (Gp_1^t, Gp_2^t, \ldots, Gp_N^t)$ and $Gg^t = (Gg_1^t, Gg_2^t, \ldots, Gg_N^t)$, respectively, represent the population activity of grid cells derived from our models and the corresponding ground truth activity. Gp_i^t is the ith grid cell's activity at time t.

In the following experiments, statistical analysis based on different sub-RNN size is done both in 2D and 3D space to arrive at more general conclusions and derive some helpful modeling instructions.

4.2.1 Grid scale

Grid cells with different spatial scales have varying sensitivity to velocity input, so the grid coding performance of sub-RNNs with different scales will differ from each other.

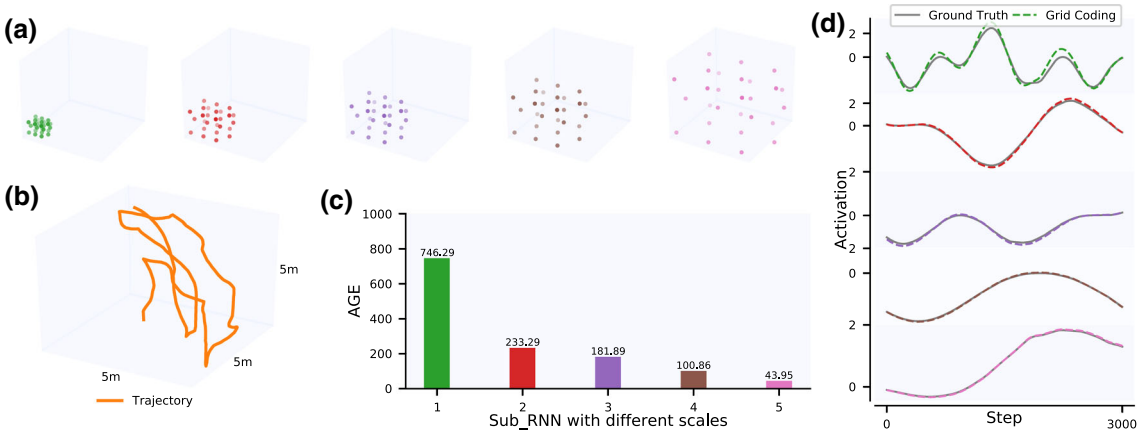

Fig. 5 Grid coding performance analysis based on different grid scales in 3D space. **a** The phase distribution of sub-RNNs with different scales. **b** The agent's exploring trajectory in a 125 m^3 area. **c** Histogram showing accumulated coding error of each sub-RNN after path integration following the simulation trajectory in **b**. **d** The comparison between the coding result derived from our model and the ground truth activity of the selected grid cells in **a**

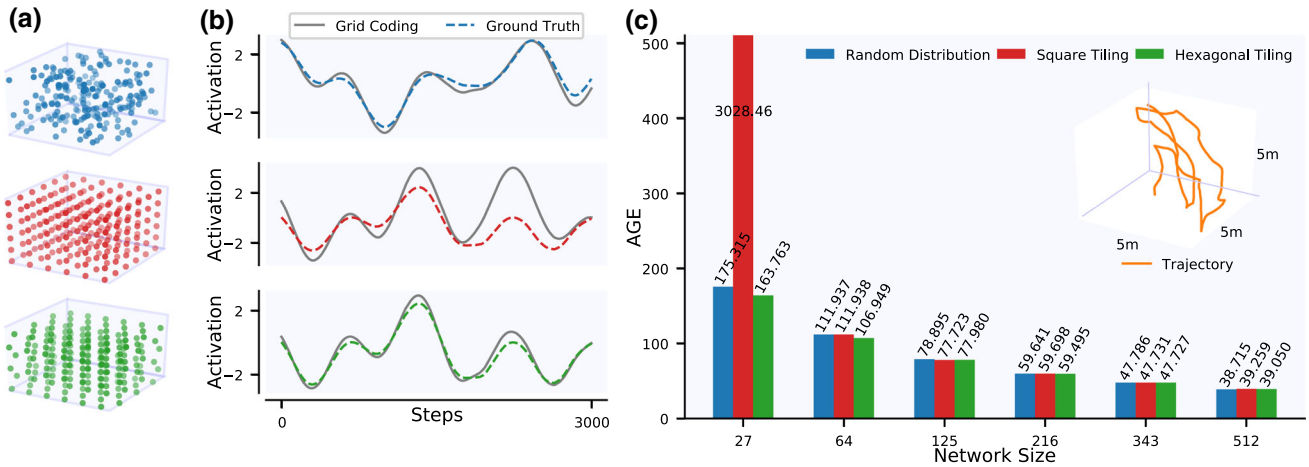

Fig. 6 Grid coding performance analysis based on different phase distributions in 3D space. **a** The phase distributions, respectively, generated by uniform random distribution, square tiling and hexagonal tiling. **b** The comparison between the ground truth and grid coding derived from our model for three grid cells randomly selected in the cases of different phase distribution. **c** Histogram showing, with different network sizes, accumulated grid coding error of the whole model in the case of different phase distributions

Signals from the same exploration trajectory (Fig. 5b) are taken as network input for analyzing the relationship between grid scale and coding performance. The phase distribution of grid cells generated by hexagonal tiling method is set for all sub-RNNs, as shown in Fig. 5a.

The activity of five grid cells from sub-RNNs with different spatial scales is recorded and compared with the ground truth activation (Fig. 5d). It can be seen that sub-RNNs with smaller scales are more sensitive to the external input and networks with larger scales are easier to keep stable grid coding performance. The statistical result of AGE for the five sub-RNNs in Fig. 5c and the experiment result in 2D space in Fig. 10 (in "Appendix 3") also demonstrate this point.

4.2.2 Grid phase

In experiment, grid cells' phases are respectively generated through random uniform distribution, square tiling and hexagonal tiling, as shown in Figs. 6a and 11a (in "Appendix 3"). For the same grid model with the same moving trajectory as input signals, we record its grid coding performance in the cases of different phase distributions, as shown in Figs. 6b and 11b (in "Appendix 3"). Furthermore, to ensure valid analysis, grid models with different network sizes are tested. As illustrated in Fig. 6c, the vertical axis represents models' AGE, while the horizontal axis represents the sub-RNN's size in models. For example, '27' means each sub-RNN includes 27 grid cells and the whole model includes 27×5 grid cells.

Statistical results in 3D and 2D space (in "Appendix 3") show that with smaller network size and fewer grid cells, the above three phase distributions vary greatly, leading to different coding performance. With the network size gradually increases, the phase distributions gradually tend to be uniform coverage, leading to similar coding performance. To be specific, the square tiling can make better coding performance only when the network size is larger, unsuitable for smaller networks while the hexagonal tiling can bring the best coding performance when the network size is smaller. Moreover, unless the uniform random distribution can make better coding performance in all cases, we won't choose it even it can bring the best coding performance in some cases. This is because principally it is an unstable method relying heavily on random seed we choose. In brief, the hexagonal tiling is a better phase generation method for grid cell modeling, which is more suitable for different network sizes and can yield better coding performance in most cases.

4.3 Path integration

Path integration is an internal computing mechanism that estimates the current location and orientation relative to an arbitrary start point by tracking distance traveled and direction changing, forming a homing vector that links the current location with the starting point [18, 27]. Accurate path integration means path integration results are required to be noise free with noise free self-motion input. Place representation and memorization for the starting and target points, a converting mechanism from self-motion to a spatial distance and a spatial information updating mechanism based on the distance are needed for completing the path integration process. There is evidence that in mammals, place representation exists in close anatomical proximity to grid cell [2]. Grid cells in adult rodents appear to function as path integrator and contribute to the neural activity of place cells[8, 34]. In this section, we first build two grid cell models in 2D and 3D space, respectively, including five sub-RNNs with different grid scales for path integration. Velocity signals from simulated trajectories are provided as network input. Sub-RNNs are projected to place cells via a linear layer for path prediction. The vector of activities in the place cells corresponding to the current

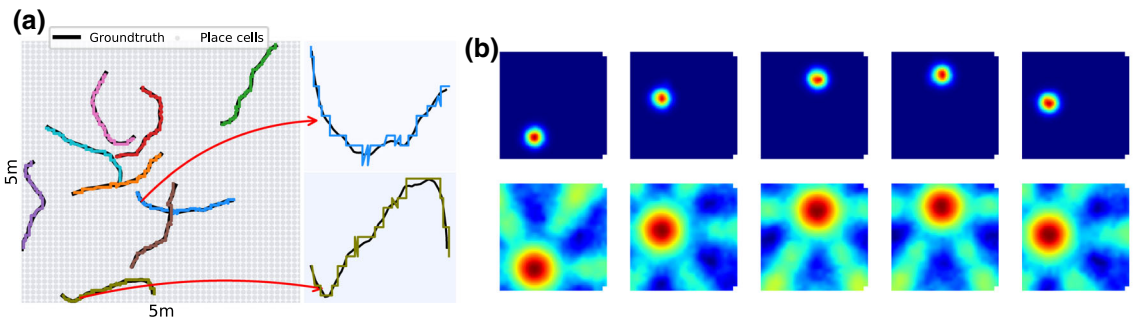

Fig. 7 Path integration in 2D space. **a** A 25 m^2 area with place cells uniformly covered during the experiment. Self-location decoded from our model (varying colors) resembles the actual path (black). **b** Top, firing fields of five place cells. Bottom, the corresponding predictive results from our model (color figure online)

position was provided as a supervised training signal at each time step.

Figures 7 and 8 show us the path integration results in a 25 m^2 2D space and a 125 m^3 3D space. To keep localization error lower than 0.25 m, 625 and 8000 place cells are set for spatial location decoding. In the grid cell models, each sub-RNN includes 216 grid cells.

As shown in Fig. 7a, with 625 place cells uniformly covering the working area, 9 trajectories are simulated. The black lines represent the ground truth, and colored lines demonstrate the path integration results. Figure 7b illustrates the ground truth activity of five place cells and the decoding results from our model. The spatial locations and the corresponding place cells can be rightly predicted and our model can execute accurate path integration.

4.4 Functioning as a metric for coding space

According to the neuroscience definition of place cell, one place cell will be only activated in one specific spatial location in an area and then represents one specific location in the area. So, when it comes to engineering modeling, it means that there must be enough place cells that can cover the agent's whole working area and ensure the spatial coding accuracy is kept at an acceptable level. As shown in Fig. 9a, for a $5 \times 5\,m^2$ 2D area, 625 place cells are needed to uniformly cover the whole area and keep the localization error within an acceptable range (here 0.2m) and for a $20 \times 20\,m^2$ 2D area, 1600 place cells are needed. However, when it comes to 3D space, 15,625 and 64,000 place cells are, respectively, needed. The huge increase in the number of place cells compared with 2D space, adding more computational burden to the system.

Neuroscience shows us that grid cells are organized in distinct modules, where each module contains grid cells with similar scale and orientation of the firing pattern [15, 29]. The joint spatial response of grid cells in only several modules is enough to generate an enormous diversity of ensemble activity because of the varying spatial scales and phases of grid cells. It is similar to the combination theory [10, 26]. Take the combination lock as an example, more than tens of thousands of unique

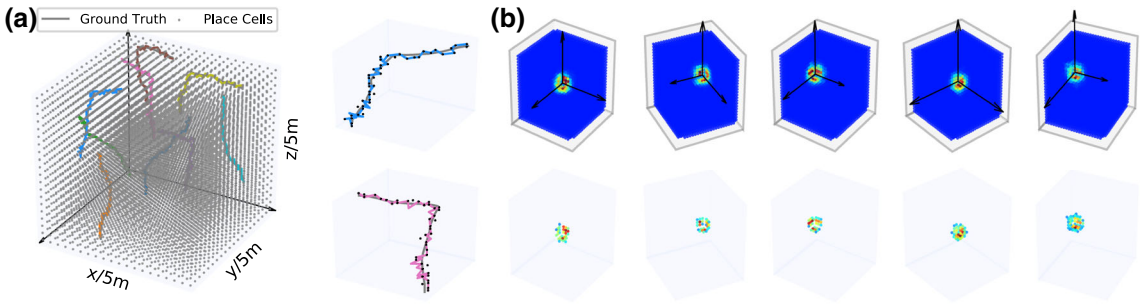

Fig. 8 Path planning of grid cells in 3D space. **a, b** Similar to Fig. 7

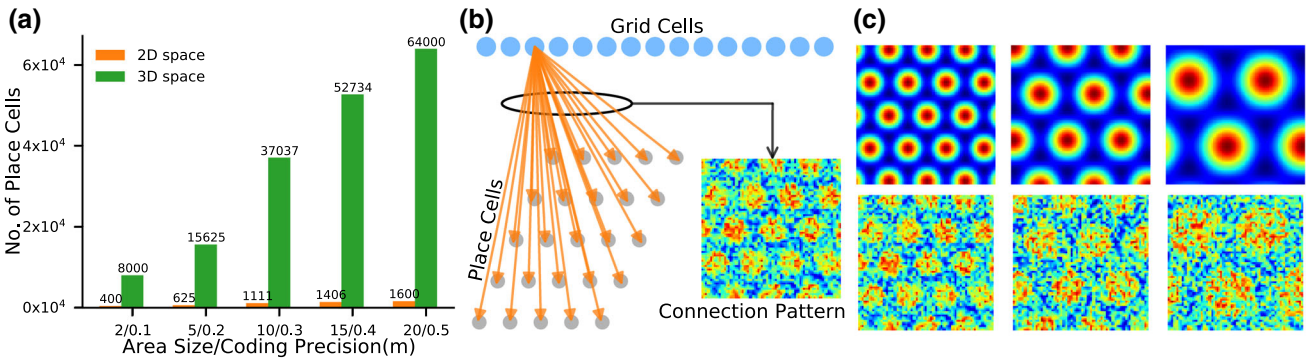

Fig. 9 Analysis about grid cells' metric ability. **a** Histogram showing the numbers of place cells needed for spatial representation in 2D and 3D spaces. **b** Schematic of the connection pattern between grid cells and place cells. **c** Top, the spatial activity maps of five grid cells with different spatial scales in our 2D grid cell model. Bottom, the connection pattern between the five grid cells to all place cells

password series can be generated by the combination of only several modules of decimal digits. The coding advantage of grid cells should be fully exerted in spatial cognition. Banino et al. [1] trained a recurrent network to perform path integration, leading to the emergence of representations resembling grid cells, furnishing agents with a Euclidean spatial metric. No details have yet been given about how grid cell functions as a metric. Here, we go a step further about the connection pattern between grid cells and place cells and do some preliminary exploration of grid cells' functioning as a metric for coding space.

According to Fig. 9b, connection patterns between grid cells and place cells are mapped as heat maps, as shown in the bottom of Fig. 9c, which exhibit spatially tuned grid-like patterns closely resembling grid cells' spatially firing patterns. If we leave noisy points in the heat maps off, then they have the same patterns with the corresponding grid cells' spatial firing patterns. It is demonstrated that grid cells embed their weighted connections to place cells into their own activity. Thus, even without the feedforward network from grid cells to place cells, the agent still can, directly based on the grid cells' population activity, decode its current spatial position and measure the spatial distance between positions at different times.

Here, we take the 2D space as an example to demonstrate the spatial decoding and distance measurement mechanism embedded in grid cells. For convenience, the agent's moving area is discretized into $N_g \times N_g$ grids and the agent's spatial position in the area can be represented as the grid index (x, y). Accordingly, spatial positions can be decoding directly from grid cells' population activity as:

$$\arg\max_{x,y}\left(\sum_{i=0}^{N} s_i GM_i\right) \tag{6}$$

where s_i is the current activity of the ith grid cell and GM_i denotes the spatial firing pattern matrix of the ith grid cell. Furthermore, the spatial distance can be measured directly from the grid cells' population activity. The agent's moving distance from time t_0 to t_1 can be measured as:

$$\delta x, \delta y = \arg\max_{x,y}\left(\sum_{i=0}^{N} s1_i GM_i\right) - \arg\max_{x,y}\left(\sum_{i=0}^{N} s0_i GM_i\right) \tag{7}$$

where $s1_i$ and $s0_i$, respectively, represent the ith grid cell's activity at time t_0 and t_1. The spatial position decoding and distance measurement in 3D space are similar to the above mechanism in 2D space.

The spatial distance metric of grid cells provides the agent with referable relative spatial relationship between the current position and historical experienced positions, which is very helpful for agent's homing behaviors that take them from the current positions directly back to the original point or historical positions.

The implication of this discovery is instructive though there is no clear conclusion about the connection between grid and place cells in neuroscience, the weight training between grid cells and place cells to furnish the agent with the ability to decode self-locations leads to grid-like connection patterns. We should ponder it from another perspective: connection weights can be seen as grid cells' contributions during spatial location decoding, which, to some extent, is spatially tuned and strongly correlated with its own firing patterns. Grid cells can function as a direct metric for coding space and do distance measurement, path planning. The exploration of the grid-like connection pattern provides a referable and instructive way of thinking about grid cells' functioning as the metric of coding space. So, learning based on neural network is a powerful tool for exploring and analyzing some underlying rules and patterns. It may will not provide direct solutions for us, but these potential rules and patterns will emerge in the learning process.

5 Conclusion

In this paper, a general grid cell modeling mechanism is given for mapping the self-motion in Euclidean space to grid cell's neural activity, achieving path integration in 1D, 2D and 3D space. Path integration is done at the network level and recurrent connections between grid cells are maintained. Different from training-based models, network weights can be worked out during the mapping process. Compared with classical CAN-based models, there is no symmetry limitation on the connection matrix and spatial representation redundancy. We go a step further based on the grid cell built following out proposed modeling mechanism. The effects of grid scale and phase on our models' grid coding performance are analyzed for deriving helpful grid cell modeling instructions to achieve accurate path integration in space of different dimensionality. In addition, the necessity of grid cells' function as a metric for coding space is underlined and an instructive and new way to explore the distance metric mechanism, few grid cells can achieve spatial encoding and distance metric for large environments, which is one of the advantages of grid

coding. The advantages of grid coding in cognitive map building and map-free navigation need to be further tapped. In addition, the necessity of grid cell's function as a metric for coding space is underlined and an instructive and new way of thinking about exploring the distance metric mechanism of grid cells. They are both the important research topics we will look further into.

Appendices

Appendix 1: Grid cell modeling in 1D space

The position in 1D space is denoted as r, which is a scalar value. There are N grid cells in the neural network and $\boldsymbol{s}(r) = [s_1(r), s_2(r), \ldots, s_N(r)]^T$(or $\boldsymbol{s} = [s_1, s_2, \ldots, s_N]^T$) represents the grid cell population activity. The formulaic description of grid cell firing patterns we used as below:

$$s_i(r) = \frac{1}{2}\cos(k_0(r - \Delta r)) + \frac{1}{2}$$

where Δr and k_0, respectively, determine the grid pattern phase and spatial scale. The weight can be calculated as follows:

$$\boldsymbol{W} = \boldsymbol{M}\boldsymbol{K}_0\boldsymbol{M}^{\dagger}$$

where

$$\boldsymbol{K}_0 = \begin{bmatrix} 0 & -k_0 \\ k_0 & 0 \end{bmatrix}$$

$$\boldsymbol{M} = \begin{bmatrix} \cos k_0\Delta r_1 & \sin k_0\Delta r_1 \\ \vdots & \vdots \\ \cos k_0\Delta r_N & \sin k_0\Delta r_N \end{bmatrix}$$

$\boldsymbol{M}^{\dagger}$ denotes the pseudo-inverse matrix of $\boldsymbol{M}$ and can be obtained through the singular value decomposition of matrix $\boldsymbol{M}$. Finally, the dynamics of grid cells in 1D space:

$$\tau \mathrm{d}\boldsymbol{s}/\mathrm{d}t = f(v_t\boldsymbol{W}\boldsymbol{s}) \tag{8}$$

where $f(x) = 0$ if $x \le 0$ otherwise $f(x) = 1$ and v_t is the moving velocity in 1D space.

Appendix 2: Grid cell modeling in 2D space

The position in 2D space is denoted as $\boldsymbol{r}$=(x, y). There are N grid cells in the neural network and $\boldsymbol{s}(\boldsymbol{r}) = [s_1(\boldsymbol{r}), s_2(\boldsymbol{r}), \ldots, s_N(\boldsymbol{r})]^T$(or $\boldsymbol{s} = [s_1, s_2, \ldots, s_N]^T$) represents the grid cell population activity. The formulaic description of grid cell firing patterns we used as below:

$$s_i(\boldsymbol{r}) = \frac{1}{3}\sum_{j=1}^{3}\cos(\boldsymbol{k}_j(\boldsymbol{r} - \Delta\boldsymbol{r})) + \frac{1}{3}$$

where $s_i(\boldsymbol{r})$ is the ith grid cell's activity. $\Delta\boldsymbol{W}$=(Δx, Δy) determines the grid pattern phase. $\boldsymbol{r}_j$ can be given as the row vector of the matrix $\boldsymbol{K}$:

$$\boldsymbol{K} = \begin{bmatrix} \boldsymbol{k}_1 \\ \boldsymbol{k}_2 \\ \boldsymbol{k}_3 \end{bmatrix} = k_0 \begin{bmatrix} \cos(\frac{\pi}{6} - \theta) & \sin(\frac{\pi}{6} - \theta) \\ \cos(-\frac{\pi}{6} - \theta) & \sin(-\frac{\pi}{6} - \theta) \\ \cos(-\frac{\pi}{2} - \theta) & \sin(-\frac{\pi}{2} - \theta) \end{bmatrix}$$

where $k_0 = 2\pi/T$. T and θ, respectively, represent the grid scale and direction, which are same for grid cells in a neural network. The weight can be calculated as follows:

$$\boldsymbol{W}^m = \boldsymbol{M}\boldsymbol{B}_m\boldsymbol{M}^{\dagger}(m = 1, 2)$$

where

$$\boldsymbol{B}_m = \begin{bmatrix} 0 & \boldsymbol{B}_{m1} \\ \boldsymbol{B}_{m2} & 0 \end{bmatrix}$$

$$\boldsymbol{B}_{m1} = diag([-K_{1m}, -K_{2m}, -K_{3m}])$$

$$\boldsymbol{B}_{m2} = diag([K_{1m}, K_{2m}, K_{3m}])$$

$$g(\Delta\boldsymbol{r}) = [\cos\boldsymbol{k}_1\Delta\boldsymbol{r} \quad \cdots \quad \cos\boldsymbol{k}_3\Delta\boldsymbol{r} \quad \sin\boldsymbol{k}_1\Delta\boldsymbol{r} \quad \cdots \quad \sin\boldsymbol{k}_3\Delta\boldsymbol{r}]$$

$$\boldsymbol{M} = \frac{1}{3}\begin{bmatrix} g(\Delta\boldsymbol{r}_1) \\ \vdots \\ g(\Delta\boldsymbol{r}_N) \end{bmatrix}$$

It should be noted that $\boldsymbol{M}^{\dagger}$ denotes the pseudo-inverse matrix of $\boldsymbol{M}$ and can be obtained through the singular value decomposition of matrix $\boldsymbol{M}$. Finally, the dynamics of grid cells in 2D space is:

$$\tau \mathrm{d}\boldsymbol{s}/\mathrm{d}t = f\left(\sum_{i=1}^{2} v_m^t\boldsymbol{W}^m\boldsymbol{r}\right) \tag{9}$$

where $f(x) = 0$ if $x \le 0$, otherwise $f(x) = 0$ and $\boldsymbol{v}_t = [v_1^t, v_2^t]^T$ is the moving velocity vector in 2D space.

Appendix 3: Grid coding performance analysis in 2D space

Grid coding performance analysis based on different grid scales in 2D space is illustrated in Fig. 10.

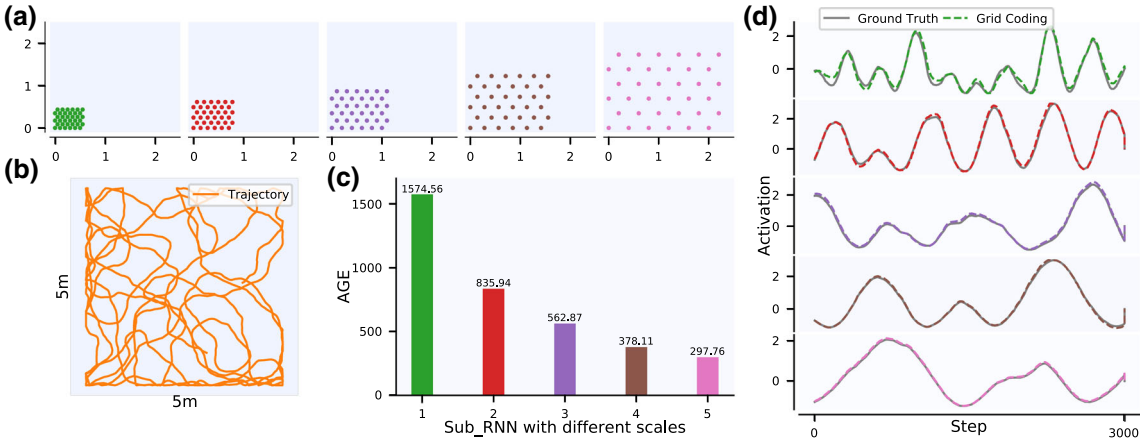

Fig. 10 Grid coding performance analysis based on different grid scales in 2D space. **a** The phase distribution of sub-RNNs with different scales. **b** The agent's exploring trajectory in a 25 m^2 area. **c** Histogram showing accumulated coding error of each sub-RNN after path integration following the simulation trajectory in **b**. **d** The comparison between the coding result derived from our model and the ground truth activity of the selected grid cells in **a**

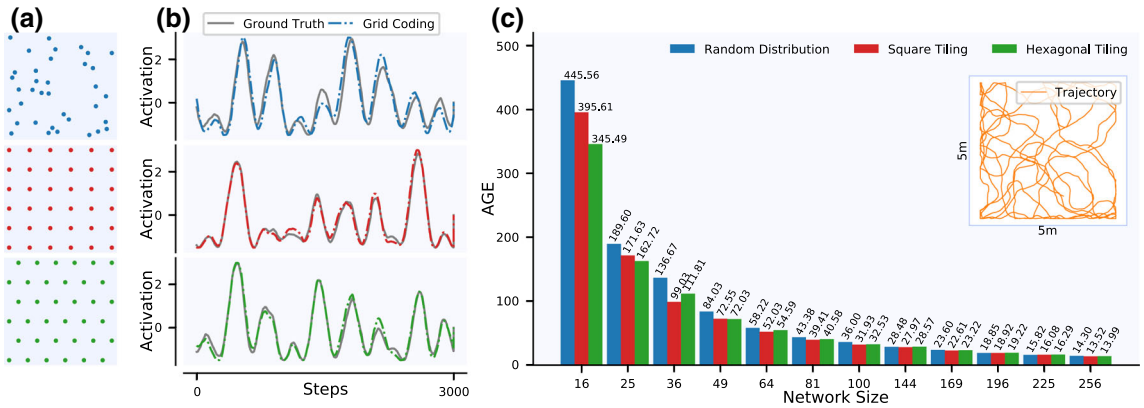

Fig. 11 Grid coding performance analysis based on different phase distributions in 2D space. **a** The phase distributions, respectively, generated by uniform random distribution, square tiling and hexagonal tiling. **b** The comparison between the ground truth and grid coding derived form our model for three grid cells randomly selected in the cases of different phase distribution. **c** Histogram showing, with different network sizes, accumulated grid coding error of the whole model in the case of different phase distributions

Grid coding performance analysis based on different phase distributions in 2D space is illustrated in Fig. 11.

Acknowledgements This work was supported by the National Natural Science Foundation of China under Grant No. 61773271 and National Natural Science Foundation of China NSAF under Grant No. U2030204.

References

1. Banino A, Barry C, Uria B, Blundell C, Lillicrap T, Mirowski P, Pritzel A et al (2018) Vector-based navigation using grid-like representations in artificial agents. Nature 557(7705):429–433
2. Barry C, Burgess N (2014) Neural mechanisms of self-location. Curr Biol 24(8):R330-339
3. Burak Y, Fiete IR (2009) Accurate path integration in continuous attractor network models of grid cells. PLOS Comput Biol 5(2):1–16
4. Burgess N, Barry C, O'Keefe J (2010) An oscillatory interference model of grid cell firing. Hippocampus 17(9):801–812
5. Bush D, Burgess N (2014) A hybrid oscillatory interference/continuous attractor network model of grid cell firing. J Neurosci 34(14):5065–5079
6. Cueva CJ, Wei XX (2018) Emergence of grid-like representations by training recurrent neural networks to perform spatial localization. In: International conference on learning representations
7. Daniel B, Caswell B, Daniel M, Neil B (2015) Using grid cells for navigation. Neuron 87(3):507–520
8. de Almeida L, Idiart M, Lisman JE (2009) The input-output transformation of the hippocampal granule cells: from grid cells to place fields. J Neurosci 29(23):7504–7512
9. Federico S, Alessandro T (2015) The self-organization of grid cells in 3d. eLife 4

10. Fiete IR, Burak Y, Brookings T (2008) What grid cells convey about rat location. J Neurosci 28(27):6858–6871
11. Fuhs MC, Touretzky DS (2006) A spin glass model of path integration in rat medial entorhinal cortex. J Neurosci 26(16):4266–4276
12. Fyhn M, Molden S, Witter MP, Moser EI, Moser MB (2004) Spatial representation in the entorhinal cortex. Science 305(5688):1258–1264
13. Gao R, Xie J, Zhu SC, Wu YN (2019) Learning grid cells as vector representation of self-position coupled with matrix representation of self-motion. In: International conference on learning representations, https://openreview.net/forum?id=Syx0Mh05YQ
14. Gil M, Ancau M, Schlesiger MI, Neitz A, Allen K, De Marco RJ, Monyer H (2018) Impaired path integration in mice with disrupted grid cell firing. Nat Neurosci 21(1):81–91. https://doi.org/10.1038/s41593-017-0039-3
15. Gu Y, Lewallen S, Kinkhabwala AA, Domnisoru C, Yoon K, Gauthier JL, Fiete IR, Tank DW (2018) A map-like micro-organization of grid cells in the medial entorhinal cortex. Cell 175(3):736-750.e30
16. Guanella A, Kiper D, Verschure P (2007) A model of grid cells based on a twisted torus topology. Int J Neural Syst 17(4):231–240. https://doi.org/10.1142/s0129065707001093
17. Hafting T, Fyhn M, Molden S, Moser MB, Moser EI (2005) Microstructure of a spatial map in the entorhinal cortex. Nature 436:801–806
18. Heinze S, Narendra A, Cheung A (2018) Principles of insect path integration. Curr Biol 28(17):R1043-1058. https://doi.org/10.1016/j.cub.2018.04.058
19. Jacobs J, Weidemann CT, Miller JF, Solway A et al (2013) Direct recordings of grid-like neuronal activity in human spatial navigation. Nat Neurosci 16(9):1188
20. Mai G, Janowicz K, Yan B, Zhu R, Cai L, Lao N (2020) Multi-scale representation learning for spatial feature distributions using grid cells. In: International conference on learning representations, https://openreview.net/forum?id=rJljdh4KDH
21. Mathis A, Herz AVM, Stemmler M (2012) Optimal population codes for space: grid cells outperform place cells. Neural Comput 24(9):2280–2317. https://doi.org/10.1162/neco_a_00319
22. Mathis A, Stemmler MB, Herz AV (2015) Probable nature of higher-dimensional symmetries underlying mammalian grid-cell activity patterns. eLife 4:e05979
23. McNaughton BL, Battaglia FP, Jensen O, Moser EI, Moser MB (2006) Path integration and the neural basis of the cognitive map. Nat Rev Neurosci 7:663–678
24. Misun K, Maguire EA (2019) Can we study 3d grid codes non-invasively in the human brain? methodological considerations and fmri findings. NeuroImage 186:667–678
25. Moser EI, Kropff E, Moser MB (2008) Place cells, grid cells, and the brain's spatial representation system. Ann Rev Neurosci 31:69–89
26. Moser MB, Rowland DC, Moser EI (2015) Place cells, grid cells, and memory. Cold Spring Harb Perspect Biol 7(2):a021808
27. Murakami H, Tomaru T, Gunji YP (2017) Interaction between path integration and visual orientation during the homing run of fiddler crabs. R Soc Open Sci 4(9):170954. https://doi.org/10.1098/rsos.170954
28. Sorscher B, Mel G, Ganguli S, Ocko S (2019) A unified theory for the origin of grid cells through the lens of pattern formation. In: Advances in neural information processing systems, vol 32, pp 10003–10013, https://proceedings.neurips.cc/paper/2019/file/6e7d5d259be7bf56ed79029c4e621f44-Paper.pdf
29. Stensola H, Stensola T, Solstad T, Fraland K, Moser MB, Moser EI (2012) The entorhinal grid map is discretized. Nature 492(7427):72–78
30. Tennant SA, Fischer L, Garden DL, Gerlei KZ, Martinez-Gonzalez C, McClure C, Wood ER, Nolan MF (2018) Stellate cells in the medial entorhinal cortex are required for spatial learning. Cell Rep 22(5):1313–1324. https://doi.org/10.1016/j.celrep.2018.01.005
31. Wei XX, Prentice J, Balasubramanian V (2015) A principle of economy predicts the functional architecture of grid cells. eLife 4:e08362. https://doi.org/10.7554/eLife.08362
32. Welinder PE, Burak Y, Fiete IR (2010) Grid cells: the position code, neural network models of activity, and the problem of learning. Hippocampus 18(12):1283–1300
33. Yartsev MM, Witter MP, Ulanovsky N (2011) Grid cells without theta oscillations in the entorhinal cortex of bats. Nature 479:103–107
34. Zhang SJ, Ye J, Miao C, Tsao A, Cerniauskas I, Ledergerber D, Moser MB, Moser EI (2013) Optogenetic dissection of entorhinal-hippocampal functional connectivity. Science 340(6128)